Heterogeneous Catalysis

Pt–Cu Core–Shell and Alloy Nanoparticles for Heterogeneous NO_x Reduction: Anomalous Stability and Reactivity of a Core–Shell Nanostructure**

Shenghu Zhou, Bindhu Varughese, Bryan Eichhorn, Greg Jackson, and Kevin McIlwrath*

Metallic nanoparticles of the noble metals find wide applications in heterogeneous gas-phase and solution-phase catalytic processes.[1–4] Small particle sizes optimize the dispersion of precious metals, such as platinum and palladium, and can also show anomalous reactivities not observed for the bulk metals. Bimetallic nanoparticles have been studied because of modified (enhanced) activities of noble metals and their abilities to catalyze multistep processes in which each metal participates in a different elementary step.[5–7] Toshima and Wang[8] first reported the synthesis of colloidal PtCu particles and showed their utility in the catalytic hydrogenation in solution. Recent studies[9,10] have suggested that supported PtCu bimetallic catalysts may be effective in NO_x reduction, but coprecipitation/impregnation methods typically used in these studies make it difficult to identify and evaluate the actual catalytic species. While some catalysts have been reported to have high activity for NO_x reduction,[11,12] the best activity and selectivity for N_2 formation (a desirable feature) is typically found with monometallic platinum catalysts.[13–15] To fully understand the catalytic activity of PtCu bimetallic catalysts and compare the activities with the monometallic materials, a detailed understanding of the composition, phase behavior, activation processes, and stabilities of the catalytic components is essential. To this end, we have embarked on a systematic investigation of the synthesis and study of bimetallic PtCu nanoparticles to evaluate their heterogeneous catalytic activities for reduction of gas phase NO with H_2 as the reducing agent.

[*] S. Zhou, B. Varughese, Prof. B. Eichhorn
Department of Chemistry and Biochemistry
University of Maryland
College Park, MD 20742 (USA)
Fax: (+1) 301-314-9121
E-mail: eichhorn@umd.edu
Prof. G. Jackson
Department of Mechanical Engineering
University of Maryland
College Park, MD 20742 (USA)
K. McIlwrath
Hitachi Instruments
Hitachi High Technologies America
5100 Franklin Drive, Pleasanton, CA 94588 (USA)

[**] This work was supported by the U.S. Department of Energy's Oak Ridge National Lab under the Advanced Reciprocating Engine Systems Program (Tim Theiss, Program Manager) and the NSF (CHE/DMR).

Supporting information for this article is available on the WWW under http://www.angewandte.org or from the author.

In addition to monometallic and alloy particles, various core–shell architectures have recently been reported, such as the gold nucleated seeded growth structures.[16–20] These nanoparticles are of interest for catalytic, optical, and magnetic applications, but their synthesis and characterization are often difficult and less studied. In particular, the synthetic routes to many target structures are challenging and the exact composition and/or phase of the resulting core and shell components are often not well understood. Systematic, detailed investigations of core–shell structures are also needed to gain a full understanding of bimetallic systems.

We report herein the synthesis and characterization of the new reciprocal core–shell structures, Pt@Cu and Cu@Pt, as well as their compositional makeup and unusual thermal stabilities. In addition, we describe a modified synthesis of PtCu alloy nanoparticles from a polyol co-reduction process and compare the thermal stability and catalytic properties with those of the core–shell structures and pure metal particles. Preliminary evaluation of γ-Al_2O_3 supported nanoparticles for catalytic NO reduction shows that the Cu@Pt nanoparticles have high activity equal to that of pure platinum nanoparticles but with significantly greater selectivity for N_2 formation.

Platinum and copper monometallic nanoparticles, PtCu alloy nanoparticles, and the Pt@Cu and Cu@Pt core–shell structures were all prepared by polyol reductions with either PVP_{55000} polymer (polyvinylpyrrolidone $M_w = 55000$) or oleylamine/oleic acid stabilizers to control particle sizes. While the individual synthetic methods are quite reproducible in producing particles of a specific size, each type of particle has a different mean particle size. Monometallic platinum and copper nanoparticles were prepared by polyol reduction of $[Pt(acac)_2]$ and $[Cu(acac)_2]$ (acac = acetylacetonate), respectively, in glycol at reflux in the presence of PVP. The mean diameters of the platinum and copper monometallic nanoparticles thus formed are 15 nm and 4 nm, respectively. An alternative method using oleylamine/oleic acid stabilizers gave much smaller platinum particles (3–7-nm particles; mean diameter 4.5 nm). Transmission electron microscopy (TEM) and X-ray diffraction (XRD) data for these materials can be found in the Supporting Information. The PtCu alloy nanoparticles were prepared by a modified version of that of Toshima and Wang[8] in which $[Pt(acac)_2]$ and $Cu(SO_4)\cdot 5H_2O$ (1:1 mole ratio) were heated at reflux in glycol with PVP to give 2–5-nm spherical particles (mean diameter 3.3 nm). Monometallic nanoparticle impurities or sulfur contamination were not detected in the PtCu samples according to TEM, XRD, EDX (energy-dispersive X-ray spectroscopy) and UV/Vis analysis. The TEM image of a representative sample is shown in Figure 1 a. The Cu@Pt nanoparticles were prepared by sequential deposition involving the reduction of $[Cu(acac)_2]$ with glycol at reflux in the presence of PVP and subsequent addition and reduction of $[Pt(acac)_2]$. TEM images showed predominately 9–10-nm hexagonal particles (mean diameter 8.8 nm) with some smaller particles of 5 nm diameter. Field emission scanning TEM (FE-STEM) phase maps qualitatively show that all particles contain platinum and copper in approximately equal quantities (Figure 1 b–d). The Pt@Cu nanoparticles were prepared in a similar fashion

 DOI: 10.1002/ange.200500919 © 2005 Wiley-VCH Verlag GmbH & Co. KGaA, Weinheim

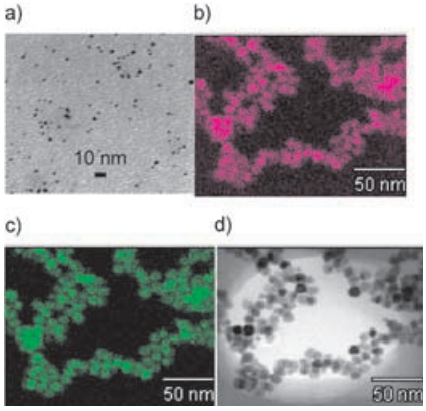

Figure 1. a) Bright-field TEM image (100 kV) of PtCu alloy nanoparticles. b–d) FE-STEM images (200 kV) of Cu@Pt nanoparticles showing b) Cu spectral map, c) Pt spectral map, and d) bright-field image.

with the initial glycol reduction of $[Pt(acac)_2]$ in the presence of PVP followed by a deposition of copper from $Cu(SO_4)\cdot 5H_2O$. FE-STEM analysis showed a broad distribution of particle sizes in the 8–20-nm size range with a mean diameter of 18.3 nm. However, all the particles again had approximately equal quantities of platinum and copper (FE-STEM phase map). A single particle EDX line scan for Cu@Pt is given in the Supporting Information. The presence of both platinum and copper in the core–shell structures is consistent with either PtCu alloys or the formation of the proposed core–shell particles. However, XRD and activity studies (see below) clearly show that the particles are not alloys. As expected, the mean diameters of each core–shell structure is larger than the diameters of the monometallic core particles.

No single analytical technique is sufficient to characterize the complex nanostructure of the core–shell particles. Comparison of several techniques is required to determine the general nature of the structure. The proposed structural models for the nanoparticle architectures described above are based on the evaluation of the combined TEM, EDX, XPS (X-ray photoelectron spectroscopy), XRD, and UV/Vis analyses. The XRD patterns of "as-prepared" PtCu alloy show the expected face-centered cubic (FCC) structure type with broad diffraction peak widths owing to the small particle sizes (mean diameter 3.3 nm, see above). After annealing the sample at 300 °C for 2 h, the peaks sharpen slightly and show 2θ peak positions[21] consistent with the target 1:1 (Pt/Cu) stoichiometry of the reaction mixture. This annealing process seems to have a dramatic effect on the catalytic activity of the particles as discussed below.

To evaluate the importance of the alloy structure in catalytic NO_x reductions, we prepared the core–shell nanoparticles Pt@Cu and Cu@Pt for comparison. The XRD data of the Pt@Cu and Cu@Pt particles are consistent with both the proposed core–shell structures and phase-separated monometallic particles. However, the FE-STEM studies described above and the activity studies (see below) are inconsistent with monometallic particles and allow us to exclude the phase-separated species from consideration. The XRD study (see Figure 2a) shows that the as-prepared Pt@Cu nanoparticles have a Pt FCC core with a $Pt_{1-x}Cu_x$ alloy shell ($x \approx 0.8$). Annealing the sample at 370 °C for 5 h converts the sample into PtCu (Figure 2b) as expected on the basis of the Pt–Cu phase diagram. In contrast, the as-prepared Cu@Pt nanoparticles have an FCC Cu core with an FCC Pt shell (Figure 2c). Surprisingly, annealing the samples at 370 °C for 5 h does not give the PtCu alloy but instead gives a Cu-rich $Pt_{1-x}Cu_x$ core and essentially a pure Pt shell (Figure 2d).

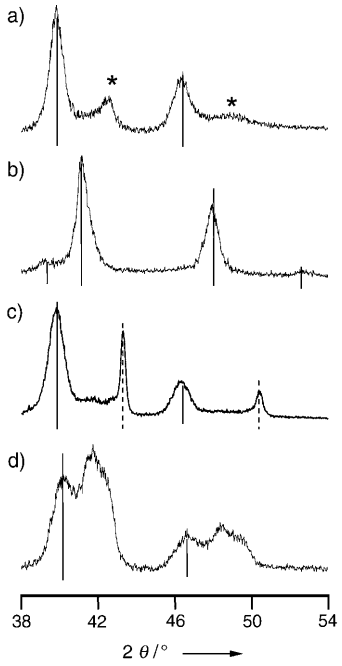

Figure 2. XRD profiles and JCPDS data (compound and file number)[21] for a) Pt@Cu (Pt, 04-0802; the asterisks indicate reflections from the $Pt_{0.2}Cu_{0.8}$ alloy), b) Pt@Cu after annealing (PtCu, 42-1326), c) Cu@Pt (Pt, 04-0802 solid vertical line; Cu, 04–0836 dashed vertical line) d) Cu@Pt after annealing (Pt, 01-1194).

We attribute this anomalous stability to Kirkendall mass-transport phenomena[22] in which the relative rates of migration of one metal into the other kinetically stabilize the Cu@Pt nanoparticles. Because the diffusion of Pt into Cu is fast (approximately $6\times10^{-7}\,cm^2h^{-1}$ at 960 °C) relative to Cu diffusion into Pt (approximately $8\times10^{-8}\,cm^2h^{-1}$ at 1041 °C),[23] the net migration at a Pt–Cu interface strongly favors Pt diffusion into the vacancies of the Cu bulk (i.e. the Kirkendall effect). In the Cu@Pt core–shell structure, the confined Cu core has a small, finite number of vacancies, which impedes net diffusion and thereby retards the alloying process. In contrast, the Cu-rich shell in the Pt@Cu nanoparticle system can maintain a high vacancy population and unhindered Pt-to-Cu diffusion. Therefore, alloying in the Pt@Cu is unimpeded but should result in a hollow PtCu alloy structure. While we know that the PtCu alloy is formed (Figure 2b), we do not yet know if the particles are hollow.

We are confident that the Pt@Cu and Cu@Pt nanoparticles are core–shell particles and not physical mixtures of monometallic components on the basis of the following experiments. 1) Annealing intimately mixed physical mixtures of Cu and Pt nanoparticles under the conditions described above does not result in alloy formation. The

 © 2005 Wiley-VCH Verlag GmbH & Co. KGaA, Weinheim

XRD profiles of the annealed physical mixture show clean peaks for FCC Cu and Pt after 5 h at 370 °C, which is in contrast to annealing behavior of both types of core–shell particles. 2) XPS spectra of the core–shell particles (Figure 3)

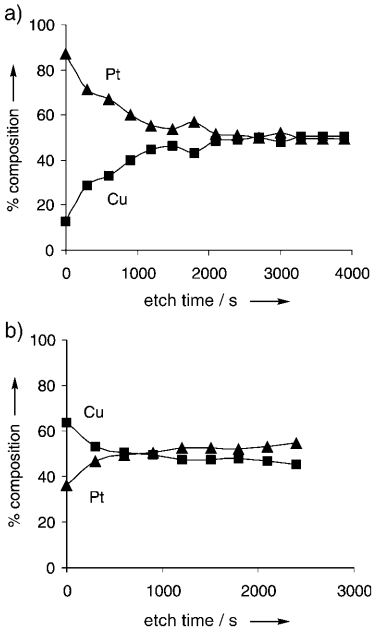

Figure 3. XPS data for a) Cu@Pt and b) Pt@Cu nanoparticles showing Pt (▲) and Cu (■) atomic percentages. Sequential Ar plasma etch sequences are shown as a function of etch time.

show atomic compositions that are highly enriched in the respective shell elements. For example, the Cu@Pt sample shows a Pt/Cu ratio of 88:12 that is indicative of a Pt-rich surface (Figure 3a). A series of 5-minute Ar plasma etches show that the composition becomes more Cu-rich as more of the particle core is exposed (or alloying takes place). After nine etches, the particles reach a 50:50 atomic ratio, which is the stoichiometric composition of the particles. The reciprocal particle, Pt@Cu, does not show the same initial large difference in surface elemental composition but achieves approximately 50:50 ratio after etching in a similar manner (Figure 3b). This behavior is consistent with the formation of the $Pt_{\approx 0.2}Cu_{\approx 0.8}$ alloy shell in contrast to a pure Cu shell and is consistent with the XRD experiments. 3) The STEM images show compositional maps that qualitatively indicate equal concentrations of each element and no monometallic particles (see Figure 1). 4) UV/Vis data show that Cu nanoparticles are not present in the colloid (no surface plasmon resonance band at around 590 nm).[1] 5) The catalytic activities of the core–shell particles are quite different to those of the monometallic particles, their alloys, and physical mixtures.

As an initial screening of the catalytic activity for NO reduction, we prepared samples of the different PtCu nanoparticles on γ-Al_2O_3 (1.06% total Pt loading) by direct deposition from colloidal suspensions. The NO conversions were evaluated by monitoring the formation of N_2, NH_3, NO_2, N_2O, and H_2O from an NO feed and H_2 reductant (0.75% NO, 3% H_2 diluted in Ar). The feed gas was passed across the catalyst (total loading, 105 mg of supported catalyst, pre-reduced in H_2) in a fixed bed reactor with a constant residence time. The reactants and products were measured (mass spectrometry) as a function of temperature. Figure 4 shows

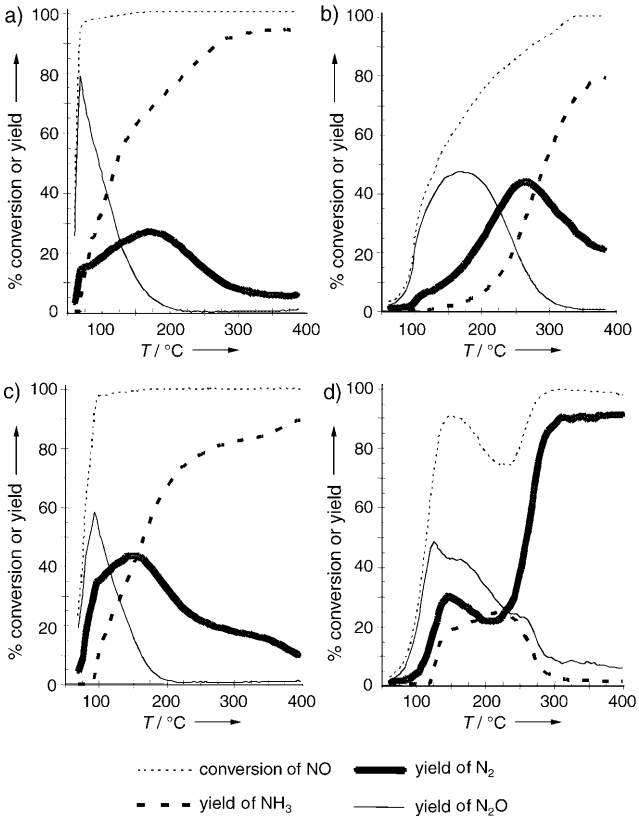

Figure 4. Temperature-programmed reactor studies of Pt–Cu bimetallic nanoparticle structures on NO reduction by H_2: a) pure Pt nanoparticles, b) PtCu alloy nanoparticles, c) Cu@Pt core–shell particles with a 4:1 ratio of H_2/NO, and d) Cu@Pt core–shell particles with a 1:1 ratio of H_2/NO. N_2 selectivity is calculated by dividing the yield of N_2 by the percentage conversion of NO.

the reactivities of a) 4.5-nm Pt, b) PtCu alloy, and c) Cu@Pt catalysts with a 4:1 ratio of H_2 to NO. The net Pt loading is the same in each. The Pt nanoparticles show a very high activity (low light off) with essentially complete NO conversion at 78 °C. However, the optimal selectivity for N_2 formation (vs. NH_3, N_2O, and NO_2) is quite low (26% at 160 °C, Figure 4a). In contrast, the PtCu alloy shows significantly better N_2 selectivity ($\approx$50% at 270 °C) but has significantly poorer activity (Figure 4b). Interestingly, the Cu@Pt core–shell nanoparticles show the high reactivity of the Pt nanoparticles and the high selectivity of the PtCu alloy (Figure 4c). For comparison, a physical mixture of Pt and PtCu alloy nanoparticles shows decreased activity and selectivity relative to the Cu@Pt core–shell system. Moreover, Pt@Cu nanoparticles show very little NO conversion under the same conditions, which is consistent with the Cu-rich shell structure (see Supporting Information).

Varying the H_2-to-NO ratio shows that the Cu@Pt core–shell catalyst can provide N_2 selectivities as high as 93% (at

 © 2005 Wiley-VCH Verlag GmbH & Co. KGaA, Weinheim

0.75% NO/0.75% H_2/98.5% Ar) over temperatures ranging from 275°C to 400°C as shown in Figure 4d. These remarkably high selectivities coincide with high NO conversion and are significantly better than the monometallic Pt systems. For example, we find 80% selectivity for the 15-nm Pt/Al_2O_3 catalyst at 400°C under identical conditions and Pt loading (see Supporting Information). These results are in good agreement with those of Burch and Coleman who reported approximately 80% selectivity for a Pt/SiO_2 catalyst (5% Pt loading) under similar conditions.[24] The 4.5-nm Pt particles show even better performance (88% selectivity at 400°C; data not shown) but are still not as selective as the Cu@Pt particles under 1:1 or 4:1 H_2/NO reaction conditions.

Further evidence of the kinetic stabilization of the Cu@Pt particles can be found in the stability tests shown in Figure 5.

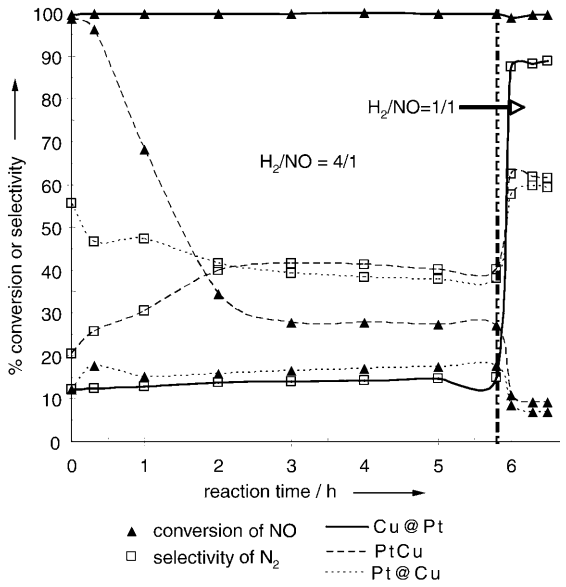

Figure 5. Stability tests for PtCu, Pt@Cu, and Cu@Pt nanocatalysts in the reduction of NO with H_2. The profiles for a 4:1 H_2/NO mixture (reaction time up to 5.8 h) are shown on the left. The subsequent reaction profiles for a 1:1 H_2/NO mixture are shown on the right.

In these experiments, NO conversion was monitored for 5.8 h at 360°C with the three different bimetallic catalysts (Cu@Pt, Pt@Cu, and PtCu) using a 4:1 H_2/NO feed. To highlight the differences in the three systems and test the thermal stability of the Cu@Pt particles under the most severe conditions, we conducted the experiments at 360°C even though the selectivity for N_2 is not optimal at these temperatures in the hydrogen-rich feed. After the 5.8-h runs, the catalysts were evaluated for NO conversion using 1:1 H_2/NO feeds for an additional 0.7 h at 360°C (Figure 5, right). For Cu@Pt, the conversion and selectivity in each feed are stable and the conversion is significantly higher than the other bimetallic systems. Post-reaction XRD analysis shows no sign of PtCu alloy formation (see Supporting Information) indicating that the particles are stable under these conditions. In contrast, the PtCu alloy catalyst rapidly loses activity (% NO conversion) but increases in N_2 selectivity during the first three hours of reaction. This change in performance is accompanied by an increase in crystallinity of the particles that may signify changes in surface structure. Interestingly, the selectivity of the Pt@Cu catalyst decreases during the first three hours and becomes equivalent to that of the PtCu alloy. This finding is consistent with the post-reaction XRD analysis that shows complete alloying of the Pt@Cu particles (see Supporting Information). The final % NO conversion of the alloyed Pt@Cu particle (17%) is lower than that of the PtCu alloy (27%), which is consistent with the significantly larger mean particle size of the Pt@Cu catalysts. Importantly, the stability and activity of the Cu@Pt nanocatalysts are markedly better than the other two bimetallic systems.

The origin of the enhanced performance of the Cu@Pt and related core–shell systems is not completely clear at present but may be related to near surface alloy (NSA) effects described by Greeley and Mavrikakis.[25] In their models, subsurface metal and alloy layers affect the binding of adsorbates (e.g. NO and H) to the particle surface. Changes in binding enthalpies can, in theory, enhance rates and selectivities in catalytic processes. Further studies designed to test these theories are in progress.

Experimental Section

The PtCu nanoparticles were prepared from $[Pt(acac)_2]$ (0.109 mmol), $Cu(SO_4)\cdot 5H_2O$ (0.109 mmol) in glycol (5 mL) with PVP_{55000} (3 mg). The solution was heated under reflux for 2 h to give a stable black colloidal suspension of PtCu nanoparticles. The Cu@Pt nanoparticles were prepared by sequential deposition involving the reduction of $[Cu(acac)_2]$ (0.156 mmol) with glycol (32 mL) and PVP_{55000} (116 mg) at reflux (20 min) to give a reddish colloidal solution. After cooling to 80°C, $[Pt(acac)_2]$ (0.156 mmol) was added and the mixture was slowly heated back to reflux (1 h) to give a black colloidal solution. The Pt@Cu nanoparticles were prepared in a similar fashion with the initial reduction of $[Pt(acac)_2]$ (0.315 mmol) in glycol (7.7 mL) at reflux for 2 h in the presence of PVP_{55000} (18.8 mg) followed by a deposition of Cu from $Cu(SO_4)\cdot 5H_2O$ (0.315 mmol) at reflux for 2 h. The 15-nm Pt particles and 4-nm Cu particles were prepared as described above but without the addition of the second metal. Smaller Pt particles (mean diameter 4.5 nm) were prepared as follows: A solution of $[Pt(acac)_2]$ (41 mg), oleic acid (133 μL; >99%), and oleylamine (133 μL; 70%, technical grade) in decahydronaphthalene (4.2 mL) was injected into decahydronaphthalene (8.3 mL) containing 1,2-hexadecanediol (83 mg; 90%, technical grade) at reflux. After 3 h under reflux, the solution was cooled to room temperature to give a black colloidal suspension of Pt nanoparticles.

Compositional phase maps were acquired using the Hitachi HD-2300 200 kV dedicated FE-STEM with an EDX detector with high sensitivity. Owing to the unique large solid angle, 2-nm spatial resolution is attainable in a relatively short time. NO reduction activity was measured by placing the supported catalyst in a packed bed arrangement in a 6.4-mm internal diameter (ID) quartz tube centered in a vertical programmable tube furnace. The catalyst charge was 5.5 mm in height. The packed bed consisted of 105 mg of catalyst (including support) intermixed with 135 mg of 1-μm quartz particles to provide adequate flow through the bed. The bed was held in place by quartz wool above and beneath, which assisted in preheating the gases to the prescribed furnace temperature. Computer-controlled electronic mass-flow controllers were used to vary flow rates and to fix reactor residence times and the reactor gas velocity (0.16 $m\,s^{-1}$). Product gases were measured continuously with a carefully calibrated magnetic sector mass spectrometer (VG Prima δB). Product compo-

 © 2005 Wiley-VCH Verlag GmbH & Co. KGaA, Weinheim

sitions were determined from the calibrated sensitivities and ion-cracking patterns for the analyzed gases.

Received: March 11, 2005

Keywords: copper · core–shell particles · heterogeneous catalysis · nanoparticles · nitrogen oxides · platinum

[1] R. M. Crooks, M. Q. Zhao, L. Sun, V. Chechik, L. K. Yeung, *Acc. Chem. Res.* **2001**, *34*, 181.
[2] Y. H. Niu, R. M. Crooks, *C. R. Chim.* **2003**, *6*, 1049.
[3] M. C. Daniel, D. Astruc, *Chem. Rev.* **2004**, *104*, 293.
[4] M. Moreno-Manas, R. Pleixats, *Acc. Chem. Res.* **2003**, *36*, 638.
[5] N. Toshima, T. Yonezawa, *New J. Chem.* **1998**, *22*, 1179.
[6] S. U. Son, Y. Jang, J. Park, H. B. Na, H. M. Park, H. J. Yun, J. Lee, T. Hyeon, *J. Am. Chem. Soc.* **2004**, *126*, 5026.
[7] R. W. J. Scott, A. K. Datye, R. M. Crooks, *J. Am. Chem. Soc.* **2003**, *125*, 3708.
[8] N. Toshima, Y. Wang, *Langmuir* **1994**, *10*, 4574.
[9] A. Obuchi, A. Ogata, K. Mizuno, A. Ohi, H. Ohuchi, *Colloids Surf. A* **1993**, *80*, 121.
[10] C. U. I. Odenbrand, J. Blanco, P. Avila, C. Knapp, *Appl. Catal. B* **1999**, *23*, 37.
[11] C. N. Costa, P. G. Savva, C. Andronikou, P. S. Lambrou, K. Polychronopoulou, V. C. Belessi, V. N. Stathopoulos, P. J. Pomonis, A. M. Efstathiou, *J. Catal.* **2002**, *209*, 456.
[12] C. N. Costa, A. M. Efstathiou, *J. Phys. Chem. B* **2004**, *108*, 2620.
[13] R. Burch, S. Scire, *Catal. Lett.* **1994**, *27*, 177.
[14] R. Burch, A. A. Shestov, J. A. Sullivan, *J. Catal.* **1999**, *186*, 353.
[15] R. Burch, A. A. Shestov, J. A. Sullivan, *J. Catal.* **1999**, *188*, 69.
[16] Y. Shiraishi, D. Ikenaga, N. Toshima, *Aust. J. Chem.* **2003**, *56*, 1025.
[17] M. S. Nashner, A. I. Frenkel, D. Somerville, C. W. Hills, J. R. Shapley, R. G. Nuzzo, *J. Am. Chem. Soc.* **1998**, *120*, 8093.
[18] N. S. Sobal, U. Ebels, H. Mohwald, M. Giersig, *J. Phys. Chem. B* **2003**, *107*, 7351.
[19] Y. Wang, N. Toshima, *J. Phys. Chem. B* **1997**, *101*, 5301.
[20] H. Yu, P. C. Gibbons, K. F. Kelton, W. E. Buhro, *J. Am. Chem. Soc.* **2001**, *123*, 9198.
[21] Powder diffraction files from the International Centre for Diffraction Data (ICDD), 12 Campus Blvd., Newtown Square, PA 19073. (http://www.icdd.com). File number 48-1549.
[22] Y. D. Yin, R. M. Rioux, C. K. Erdonmez, S. Hughes, G. A. Somorjai, A. P. Alivisatos, *Science* **2004**, *304*, 711.
[23] A. K. Sinha, *Physical Metallurgy Handbook*, McGraw-Hill, New York, **2003**.
[24] R. Burch, M. D. Coleman, *J. Catal.* **2002**, *208*, 435.
[25] J. Greeley, M. Mavrikakis, *Nat. Mater.* **2004**, *3*, 810.

 © 2005 Wiley-VCH Verlag GmbH & Co. KGaA, Weinheim